Monthly Notices of the ROYAL ASTRONOMICAL SOCIETY

MNRAS **486,** 4686–4700 (2019) doi:10.1093/mnras/stz1029
Advance Access publication 2019 May 4

The morphology and kinematics of the gaseous circumgalactic medium of Milky Way mass galaxies – II. Comparison of IllustrisTNG and Illustris simulation results

Guinevere Kauffmann,[1]★ Dylan Nelson,[1] Sanchayeeta Borthakur,[2] Timothy Heckman,[3] Lars Hernquist,[4] Federico Marinacci,[5] Rüdiger Pakmor[1] and Annelisa Pillepich[6]

[1]*Max-Planck Institut für Astrophysik, Karl-Schwarzschild-Straße 1, D-85741 Garching, Germany*
[2]*School of Earth and Space Exploration, Arizona State University, Tempe, AZ D-85287, USA*
[3]*Department of Physics and Astronomy, Center for Astrophysical Sciences, Johns Hopkins University, Baltimore, MD 21218, USA*
[4]*Harvard-Smithsonian Center for Astrophysics, 60 Garden Street, Cambridge, MA 02138, USA*
[5]*Kavli Institute for Astrophysics and Space Research, Massachusetts Institute of Technology, Cambridge, MA 02139, USA*
[6]*Max-Planck-Institut fr Astronomie, Knigstuhl 17, D-69117 Heidelberg, Germany*

Accepted 2019 April 9. Received 2019 April 4; in original form 2018 December 17

ABSTRACT

We have carried out a controlled comparison of the structural and kinematic properties of the circumgalactic medium (CGM) around Milky Way mass galaxies in the Illustris and IllustrisTNG simulations. Very striking differences are found. At $z = 0$, gas column density and temperature profiles at large radii ($\sim$100 kpc) correlate strongly with disc gas mass fraction in Illustris, but not in TNG. The neutral gas at large radii is preferentially aligned in the plane of the disc in TNG, whereas it is much more isotropic in Illustris. The vertical coherence scale of the rotationally supported gas in the CGM is linked to the gas mass fraction of the galaxy in Illustris, but not in TNG. A tracer particle analysis allows us to show how these differences can be understood as a consequence of the different subgrid models of feedback in the two simulations. A study of spatially matched galaxies in the two simulations shows that in TNG, feedback by supernovae and active galactic nuclei (AGNs) helps to create an extended smooth reservoir of hot gas at high redshifts, which then cools to form a thin, rotationally supported disc at later times. In Illustris, AGNs dump heat in the form of hot gas bubbles that push diffuse material at large radii out of the halo. The disc is formed by accretion of colder, recycled material, and this results in more vertically extended gas distributions above and below the Galactic plane. We conclude that variations in the structure of gas around Milky Way mass galaxies are a sensitive probe of feedback physics in simulations and are worthy of more observational consideration in future.

Key words: galaxies: formation – galaxies: haloes – galaxies: structure.

1 INTRODUCTION

The thin stellar disc of our Milky Way is believed to have formed over the last 9 Gyr, i.e. since a redshift of $\sim$1, making it the youngest stellar component of our Galaxy (see Rix & Bovy 2013, for a recent review). The current ongoing star formation in the Milky Way would exhaust the available molecular gas supply in just 1–2 Gyr, which means that disc gas must be replenished from an outer reservoir. Outer gas reservoirs may exist in the form of an extended disc of atomic gas at lower densities, or as diffuse gas in a more spherical halo that cools and accretes on to the main disc over time (Bauermeister, Blitz & Ma 2010).

Studies of the circumgalactic medium (CGM) around galaxies provide a means of understanding gas accretion processes in more detail. The CGM is generally defined as gas that is outside the main disc of a galaxy, but within the virial radius of its surrounding dark matter halo. In our own Milky Way and in the most nearby galaxies, it is possible to study individual clouds in the CGM (see Putman, Peek & Joung 2012, for a review). In more distant galaxies, the gas may either be observed in absorption, most commonly in the spectra of high-redshift quasars whose sightlines pass within a few hundred kiloparsecs of a galaxy at lower redshift (e.g. Zhu et al. 2014), or in emission in the form of X-ray emitting gas at high temperatures, as

★ E-mail: gamk@mpa-garching.mpg.de

extra-planar, diffuse ionized gas around low-redshift galaxies (e.g. Jones et al. 2017), or as giant Ly α emitting haloes around quasars at high redshifts (Martin et al. 2016; Arrigoni-Battaia et al. 2018). One major complication in the interpretation of such observations is that CGM gas is likely to consist of a mixture of outflowing gas that has been heated by supernovae in the disc, and inflowing gas that will fuel future star formation.

The interplay between inflowing and outflowing gas on CGM observables can be studied using simulations of galaxy formation that calculate the hydrodynamical evolution of gas under the influence of the gravitational field of an evolving dark matter density field in cosmological volumes of the Universe. These simulations have now reached sufficient particle number and mass resolution to track the formation and evolution of hundreds of galaxies of Milky Way mass within volumes of 100 Mpc^3 with spatial resolution of around 1 kpc (e.g. Dubois, Volonteri & Silk 2014; Genel et al. 2014; Vogelsberger et al. 2014a; Khandai et al. 2015; Nelson et al. 2015a; Schaye et al. 2015). Recent work has demonstrated that the radial extent and covering fraction of Ly α and metal absorption line gas are extremely sensitive to the detailed implementation of feedback from supernovae and active galactic nuclei (AGNs) in numerical hydrodynamical models (Suresh et al. 2015). This is particularly true of tracers of transient warm gas, such as O VI, which are sensitive probes of recent energy ejection processes (Nelson et al. 2018b).

Attempts to use CGM observables to elucidate gas accretion mechanisms are less advanced. Stewart et al. (2011) (see also Danovich et al. 2015) suggested high angular momentum gas corotating with the galactic disc as a clear and unambiguous signature of cosmological gas accretion on to galaxies. Their analysis of simulations of Milky Way mass galaxies at $z = 2$ suggested that the corotating material would form a thickened, warped extended structure that should be detectable as background object absorption lines offset from the central galaxy's systemic velocity in a single direction. Evidence has been found that the population of Mg II absorbers located close to the galactic disc plane have Doppler shifts with the same sign as the galactic rotation, lending credence to this picture (Kacprzak, Churchill & Nielsen 2012; Ho et al. 2017; Martin et al. 2019). The kinematics of gaseous haloes around quasars can be studied in considerable detail, because the strong radiation field emitted by the accreting black hole ionizes the gas out to large distances (Liu et al. 2013). Integral field unit spectroscopy of Ly α emitting haloes around quasars at redshift 2–3 has revealed large-scale coherent rotation-like patterns spanning 300 $\mathrm{km\,s^{-1}}$ with a large velocity dispersion, which are interpreted as a signature of the inspiralling accretion of substructures within the quasar's host halo (Arrigoni-Battaia et al. 2018).

Although it has been argued that high angular momentum CGM gas corotating with the disc is a generic qualitative prediction of the Λ Cold Dark Matter cosmological paradigm (Stevens et al. 2017; Stewart et al. 2017; Oppenheimer 2018), it is not yet understood how robustly simulations can predict the detailed morphology, kinematics, and temperature structure of this gas, and how such properties are expected to vary as a function of galaxy properties.

Kauffmann, Borthakur & Nelson (2016, hereafter KBN16) carried out a comparison of the CGM for galaxies with different disc cold gas mass fractions using the Illustris simulations. This was motivated by the observational findings of Borthakur et al. (2015), showing strong correlation (99.8 per cent confidence) between the gas fraction of the galaxy and the impact-parameter-corrected Ly α equivalent width of absorbers in the spectra of background quasi-stellar objects at impact parameters of 63–231 kpc. KBN16 found that the Illustris neutral hydrogen column densities in the CGM increased as a function of disc gas mass fraction out to radii of 100 kpc. The neutral hydrogen was found to rotate coherently about the centre of the galaxy with a maximum rotational velocity of around 200 $\mathrm{km\,s^{-1}}$. In gas-rich galaxies, the average *vertical* coherence length of the rotating gas was 40 kpc, compared to only 10 kpc in gas-poor galaxies.

In this paper, we test the robustness of these results to changes in the subgrid models for supernovae and AGN feedback by undertaking an identical analysis for the new IllustrisTNG simulation. We find that clear trends in CGM properties with disc gas mass fraction are almost entirely absent in IllustrisTNG. In order to understand why the two simulations give such different results, we carry out an analysis of the heating/cooling and inflow/outflow patterns of circumgalactic gas as a function of radius in the halo for a set of Milky Way mass galaxies with different disc gas mass fractions. Because the two simulations are run using identical initial conditions, we can carry out the analysis for a spatially matched set of haloes, thus eliminating differences that may arise as a result of different halo formation histories. In addition, we note that the two simulations are carried out using the same code AREPO (Springel 2010), thus eliminating differences due to different numerical schemes.

Our paper is organized as follows. In Section 2, we summarize the main changes to the physical prescriptions between the Illustris and IllustrisTNG simulations relevant for this study. In Section 3, we directly compare the radial profiles, morphology, and rotational kinematics of the gas in the two simulations in three bins of disc gas mass fraction. In Section 4, we describe how tracer particles can be used to track the temperature evolution and motions of gas between different simulation snapshots. We present a comparison of how heating/cooling as well as inflow/outflow patterns differ between matched galaxies in the two simulations. In Section 5, we summarize our main results and attempt to elucidate how and why changes to the feedback prescriptions lead to very different CGM structure and morphology around present-day galaxies.

2 SIMULATIONS AND SAMPLES

We analyse two simulations herein. First, we make use of data from the Illustris-1 simulation (Vogelsberger et al. 2014a,b; Genel et al. 2014), the highest resolution of the publicly released simulation boxes with a volume of $10^{6.5}$ Mpc^3, dark matter and gas particle masses of 6.3×10^6 and $1.6 \times 10^6\,\mathrm{M}_\odot$, respectively, and dark matter and gas gravitational softening lengths of 1.4 and 0.7 kpc, respectively. Secondly, we include simulations from the IllustrisTNG project (Marinacci et al. 2018; Naiman et al. 2018; Nelson et al. 2018a; Pillepich et al. 2018; Springel et al. 2018), which includes three distinct simulation volumes: TNG50, TNG100, and TNG300. Here, we make use of TNG100, for which the baryon mass resolution is $1.4 \times 10^6\,\mathrm{M}_\odot$. For the complete numerical details about this run, see table A2 of Nelson et al. (2018a). An overview of the differences between the TNG galaxy formation physics model and the original Illustris simulation model, including the fiducial values of all parameters, is given in table 1 of Pillepich et al. (2018). The main differences that are likely to impact the CGM are differences in the treatment of galactic winds and black hole feedback, so we briefly summarize them here.

2.1 Galactic winds

In TNG, wind particles are launched isotropically, rather than in a direction perpendicular to the disc. Tests show that this change

has little influence on the morphology of the galactic wind (fig. 5 of Pillepich et al. 2018). The change that is likely to impact CGM properties most strongly is the revised scaling of the wind particle speed with galaxy/halo properties. In Illustris, the wind particle speed is assumed to scale with the local, one-dimensional dark matter velocity dispersion – the prescription follows the implementation of feedback in Oppenheimer & Davé (2006). In IllustrisTNG, the wind speed is assumed to scale not only with $\sigma_{\rm DM}$ but also with redshift, in such a way that the wind speed is redshift-independent at fixed halo mass. Unlike Illustris, TNG also includes a minimum wind velocity, so that the wind injection speed never drops below 350 km s^{-1} in any halo at any redshift. This increases the effectiveness of feedback in low-mass galaxies and at higher redshifts. Wind mass-loading factors also evolve in opposite directions at fixed halo mass in TNG and Illustris. Finally, in addition to the changes in wind injection velocity, TNG includes two additional changes affecting how the available wind energy is distributed: (i) some given fraction of this energy is thermal and (ii) the wind energy depends on the metallicity of the star-forming gas cell, such that galactic winds are weaker in higher metallicity environments. In a dark matter halo of $\sim 10^{12}$ M$_\odot$, this means that the wind mass-loading factors at injection are the same in Illustris and IllustrisTNG at $z \sim 2$–3, but a factor of 2 lower in TNG at $z = 0$.

In summary, for Milky Way-type haloes, galactic winds have similar properties in the two simulations at high redshifts, but at low redshifts, TNG winds are injected with higher velocities, but with lower mass-loading factors.

2.2 Black hole feedback

Both Illustris and IllustrisTNG include two modes of AGN feedback. The mode operating at high accretion rates, the so-called quasar mode, is similar in the two simulations. A fraction of the radiative energy released by the accreted gas couples thermally to nearby gas within a radius that contains some fixed amount of mass. For low-activity states of the black hole, a 'bubble model', a form of mechanical radio-mode AGN feedback following Sijacki et al. (2007) is implemented in Illustris. Bubbles of hot gas with a radius $\sim$50 kpc and total energy $\sim 10^{60}$ erg and volume density $\sim 10^4$ M$_\odot$ kpc^{-3} are placed into the halo at distances of $\sim$100 kpc from their centres. The radio-mode feedback efficiency provided by the bubbles is assumed to be a fixed fraction of the rest-mass energy of the gas accreted by the black hole. The main problem with this model, as implemented in Illustris, was that a significant fraction of the gas in haloes of masses of the order of 10^{13} M$_\odot$ was expelled beyond the virial radius of the halo by the present-day, violating constraints on the observed X-ray luminosities of groups and clusters (Genel et al. 2014). In addition, the Illustris bubble model did not quench ongoing star formation in the central galaxies of massive haloes. These problems motivated a switch to a kinetic feedback model in IllustrisTNG (Weinberger et al. 2017).

In both Illustris and IllustrisTNG, the Eddington ratio is used as the criterion for deciding the accretion state of the black hole. IllustrisTNG includes an additional dependence on black hole mass that acts to push massive black holes into the kinetic mode at higher Eddington ratios compared to lower mass black holes. The 'pivot' black hole mass where the kinetic mode becomes dominant is around 10^8 M$_\odot$. Unlike in the high-accretion state, momentum but no thermal energy is input into gas cells in the neighbourhood of the black hole. Note that the momentum is added in a random direction when averaged in time across multiple feedback events – surprisingly, the kinetic mode at low Eddington rates does produce coherent gas flows, as might be expected in the case of a large-scale relativistic jet interacting with the CGM (see Nelson et al. 2019). As in the bubble feedback model, the kinetic feedback mode is discretized by imposing a minimum energy that needs to accumulate before the feedback energy is released. The adopted energy threshold is assumed to scale with the square of the dark matter velocity dispersion multiplied by the gas mass in the feedback region. This scaling was chosen to ensure that in IllustrisTNG, the specific energy of the AGN wind within individual injections did not significantly exceed the specific binding energy of the halo, resulting in minimal gas escape from the halo and changes to the thermodynamic state of the gas on large scales.

2.3 Magnetic fields

We note that another addition in the TNG model is the inclusion of magnetic fields (Pakmor, Bauer & Springel 2011). Galaxies in runs with and without magnetic fields have been found to differ somewhat in their gas masses and sizes (Pillepich et al. 2018). Within the disc, magnetic fields appear to have little dynamical impact on structures such as spiral arms, bulges, and bars (Pakmor & Springel 2013; Pakmor et al. 2017). The impact of the magnetic field on the structure of the CGM has not yet been examined in detail.

2.4 Samples

We now describe the two samples of haloes analysed in this paper. The first of these is used to generate Figs 1–6 and pertain to the analysis of the statistical properties of the CGM as a function of galaxy gas mass fraction. The second sample is used for the comparative analysis of gas flows and heating/cooling, and is used to generate Figs 7–14.

2.4.1 Statistical analysis of CGM properties as a function of galaxy gas mass fraction

The analysis of Milky Way-type galaxies in KBN16 focused on a sample of galaxies with stellar masses (calculated within twice the half-mass radius) in the range (6–8) $\times$ 10^{10} M$_\odot$ residing in subhaloes with dark matter masses in the range (1–2) $\times$ 10^{12} M$_\odot$. The sample was divided into four bins in gas mass fraction $f_{\rm g} = M_{\rm gas}/M_{\rm stars}$, where $M_{\rm gas}$ was again evaluated within twice the stellar half-mass radius. The $f_{\rm g}$ ranges were 0.01–0.03, 0.03–0.1, 0.1–0.3, and 0.3–1.

Fig. 1 shows the gas mass fraction distributions of Illustris galaxies compared to IllustrisTNG galaxies in four different ranges of stellar mass. As in KBN16, both the gas and the stellar mass are evaluated within twice the stellar half-mass radius. There has been no attempt to split the total gas into atomic, molecular, and ionized components as in Diemer et al. (2018) and Stevens et al. (2019) – the comparison here is between the two simulations. An attempt to assess the match with observations using a sample of galaxies with both atomic and molecular gas measurements is presented in fig. 1 of KBN16, where it was found that the simulations yield too many very gas-rich galaxies at Milky Way masses (3×10^{10}–10^{11} M$_\odot$).

As can be seen, the gas mass fraction distributions in the two simulations differ most strongly in this mass range; the fraction of galaxies with gas mass fractions less than 0.01 reaches values in excess of 0.5 in IllustrisTNG compared to only a

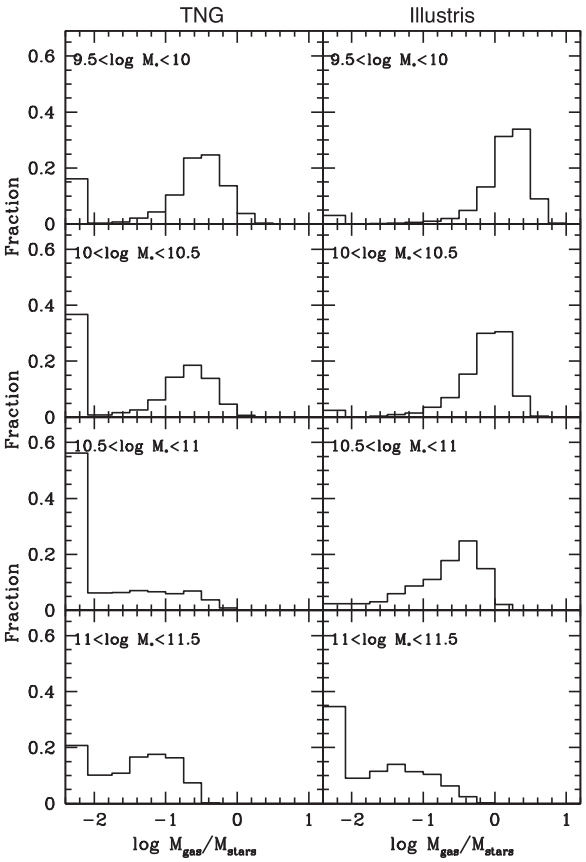

Figure 1. Black histograms show total gas mass fractions evaluated within twice the stellar half-mass radius for galaxies in the IllustrisTNG (left) and Illustris (right) simulations. Results are shown in four different stellar mass bins.

few per cent in Illustris, and there are very few galaxies in IllustrisTNG with gas mass fractions close to 1. This is because almost all galaxies in this stellar mass range have black holes with masses of around $10^8\,M_\odot$. In IllustrisTNG, AGN kinetic feedback kicks in very strongly at this black hole mass and AGN feedback prescriptions are thus maximized for Milky Way mass systems (see Weinberger et al. 2018). We thus regard the 3×10^{10}–$10^{11}\,M_\odot$ stellar mass range as ideal for looking for observational tests of the differences in the feedback prescriptions. At the same time, we caution that a black hole mass of $10^8\,M_\odot$ is too large for disc-dominated galaxies like the Milky Way by a factor of 3–10 (Genzel, Eisenhauer & Gillesen 2010). This would imply that the effects of black hole feedback are simply too dominant in TNG Milky Way-type galaxies.

The strong differences at the Milky Way mass scale also cause problems for making robust systematic comparisons between Illustris and IllustrisTNG as a function of galaxy gas mass fraction. In order to sample a wide range in gas mass fraction in both simulations, we adopt slightly different stellar mass and halo mass cuts for the two. For Illustris, we select galaxies with stellar masses in the range $10.6 < \log M_* < 10.8\,M_\odot$ and halo masses in the range $12.0 < \log M_{\rm halo} < 12.3\,M_\odot$, very similar to the cut in KBN16. For IllustrisTNG, we lower the stellar and halo mass limits slightly, and select galaxies with stellar masses in the range $10.4 < \log M_* < 10.7\,M_\odot$ and halo masses in the range $11.7 < \log M_{\rm halo} < 12.3\,M_\odot$. We only carry out the comparison for 3 bins in $f_{\rm g}$: 0.03–0.1, 0.1–0.3, and 0.3–1, for which there are more than 20 subhaloes in each bin in both the simulations. We note that galaxies in the highest gas fraction bin will be slightly less massive in IllustrisTNG than in Illustris, but we believe that the adopted mass ranges are similar enough that the comparison is still meaningful. We also note that the stellar mass-to-halo mass relation is modified in TNG compared to Illustris (see fig. 11 of Pillipich et al. 2018), with TNG lower at fixed halo mass at the mass scale of Milky Way-type galaxies, so the offset adopted here is within the systematic differences in the calibration of the two simulations.

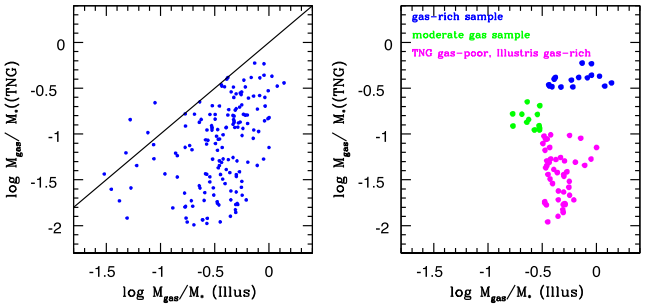

Figure 2. Left: The full sample of matched subhaloes. The gas fraction of the galaxy in IllustrisTNG is plotted as a function of the gas fraction of its Illustris analogue. A one-to-one line is drawn to guide the eye. Right: The subsamples that are studied in this paper (see the text).

2.4.2 *Matched halo analysis*

In order to understand differences in the dynamics (inflow/outflow) and thermodynamic state of the CGM in the two simulations, we apply a matching algorithm to identify pairs of analogue subhaloes across the two simulations. Counterparts are identified using the Lagrangian region matching algorithm of Lovell et al. (2014). The initial conditions for a Lagrangian patch of each halo are determined using the dark matter particles that the subhalo has at the snapshot at which it achieves its maximum mass. The Lagrangian patch is then compared to the patches of haloes in the companion simulation by means of their density distributions and gravitational potentials to obtain a quality-of-match statistic. The companion simulation subhalo with the highest value of this statistic is then considered the 'match'. We have selected a set of 169 matched subhaloes using method (2) with masses in the range (6×10^{11})–$(2 \times 10^{12})\,M_\odot$ that contain galaxies with stellar masses in the range 5×10^{10}–$10^{11}\,M_\odot$ with gas mass fractions larger than 0.01.

The full sample is shown in the left-hand panel of Fig. 2. We plot the gas fraction of the galaxy in IllustrisTNG as a function of the gas fraction of its Illustris analogue. In the right-hand panel, we define a set of subsamples for further study: (1) a set of galaxies with $f_{\rm gas} > 0.3$ in both Illustris and IllustrisTNG (hereafter, the gas-rich sample), (2) a set of galaxies with $0.1 < f_{\rm gas} < 0.3$ in both simulations (hereafter, the moderate gas sample), and (3) a set of galaxies with $f_{\rm gas} < 0.1$ in the IllustrisTNG simulation and $f_{\rm gas} > 0.1$ in Illustris (hereafter, gas-poor TNG galaxies). We note that we could have defined a set of galaxies with $f_{\rm gas} < 0.1$ in both simulations, but further examination revealed that all such cases in Illustris are actually satellite subhaloes. In these systems, environmental processes such as ram-pressure stripping affect the CGM in addition to processes such as cooling, and supernovae and AGN feedback. Because of this extra degree of

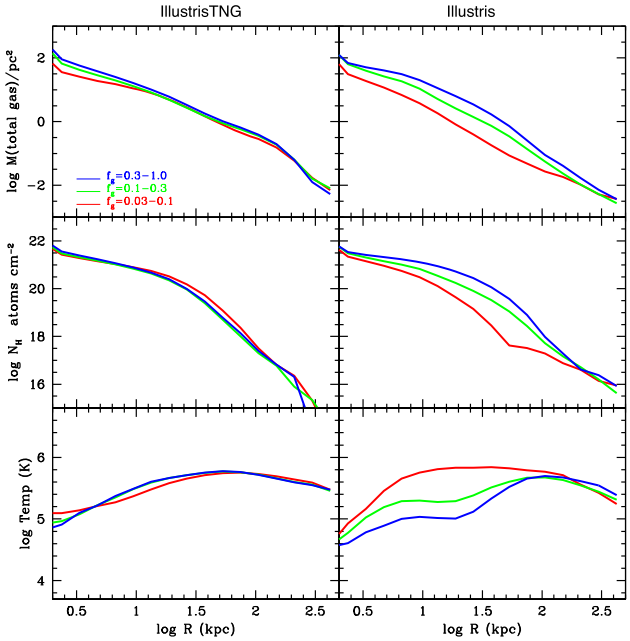

Figure 3. The mean radial distribution of the logarithm of the total gas density, neutral gas column density, and gas mass-weighted temperature as a function of radius from the centre of the subhalo. Results are shown for IllustrisTNG in the left-hand panels and for Illustris in the right-hand panels. The red, green, and blue curves show results for the samples with f_g in the ranges 0.03–0.1, 0.1–0.3, and 0.3–1, respectively.

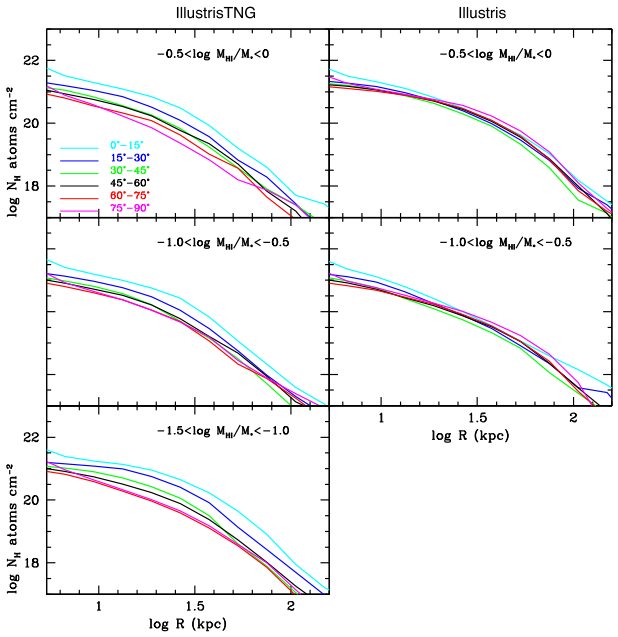

Figure 4. Different colour lines show radial profiles of neutral hydrogen column density evaluated at different orientation angles with respect to the major axis of the disc: 0°–15° (cyan), 15°–30° (blue), 30°–45° (green), 45°–60° (black), 60°–75° (red), and 75°–90°(magenta). Results are shown for IllustrisTNG in the left column and for Illustris in the right column. Results for galaxies in different gas fraction ranges are plotted in different rows.

complexity, we do not consider galaxies in this regime of parameter space.

3 CGM STRUCTURE TRENDS AS A FUNCTION OF GALAXY GAS FRACTION

In this section, we present a comparison of the radial profiles of the gas, as well as probes of gas morphology, asymmetry, and the coherent rotation of the CGM for galaxies as a function of gas mass fraction in Illustris and IllustrisTNG. Computational methodologies, results for the Illustris simulation, and some comparison with available observational data were discussed in detail in KBN16, and the reader is referred to sections 3.2–3.5 and 4 of that paper for details. Here, we focus on the comparison between the two models.

Fig. 3 shows the mean radial distribution of the logarithm of the total gas density, neutral gas column density, and gas mass-weighted temperature as a function of radius from the centre of the subhalo. Results are shown for IllustrisTNG in the left-hand panels and for Illustris in the right-hand panels. The red, green, and blue curves show results for the samples with f_g in the ranges 0.03–0.1, 0.1–0.3, and 0.3–1, respectively. The gas masses, neutral hydrogen fractions, and gas temperatures for each cell are read directly from the simulation outputs. As can be seen, the radial distributions of all three quantities depend strongly on galaxy gas mass fraction out to radii of 70–100 kpc in the Illustris simulation. Gas-rich galaxies are surrounded by a higher density, cooler CGM on average than gas-poor galaxies. The same is not true, however, in IllustrisTNG. The average densities and temperature of the CGM on scales larger than 10 kpc do not depend on the gas fraction of the galaxy.

Fig. 4 explores the extent to which the CGM gas is aligned positionally with the disc of the galaxy. Different colour lines show radial profiles of neutral hydrogen column density evaluated at different orientation angles with respect to the major axis of the disc. Results are shown for IllustrisTNG in the left column and for Illustris in the right column. Results for galaxies in different gas fraction ranges are plotted in different rows. As discussed in KBN16, there is no clear alignment of the CGM neutral gas in the plane of the disc in the Illustris simulation for the more gas-rich systems. In IllustrisTNG, we do see a clear trend for the average neutral gas density to be larger when measured in the plane of the disc. The systematic boost in $\log N_H$ reaches a factor of 10 and is present out to distances of 100 kpc.

In KBN16, we defined a set of asymmetry indices that we designed to probe the average asymmetry of the CGM, both above and below the galactic plane, and on either side of the disc. To measure these indices, the galaxy was first rotated into its edge-on configuration. Radii along the major axis $R_x(90)$, $R_x(95)$, and $R_x(99)$ enclosing 90, 95, and 99 per cent of the in-plane projected stellar mass were measured. The asymmetry indices A_c (up–down 90), A_c (up–down 95), A_c (up–down 99), A_c (right–left 95), and A_c (right–left 99) were defined, where 'up–down' means above and below the galactic place, and 'right–left' means on either side of the disc minor axis. To compute the indices, we integrate up the total gas columns from a scale height of 2 kpc above/below the plane out to a distance of 200 kpc, and compute (for example) A_c (up–down 90) as $\log([M_{tot}(up) - M_{tot}(down)]/[M_{tot}(up) + M_{tot}(down)])$, i.e. the index is expressed in terms of the logarithm of the fractional difference in total gas mass above and below the central disc. The other four indices are defined in similar fashion.

Fig. 5 compares the distributions of some of these indices in the two simulations. Results for IllustrisTNG are shown in the top row and in the bottom row for Illustris. The red histograms are for gas-poor galaxies with $f_g = 0.03$–0.1, while the blue histograms are for gas-rich galaxies with $f_g = 0.3$–1. In Illustris, gas-poor

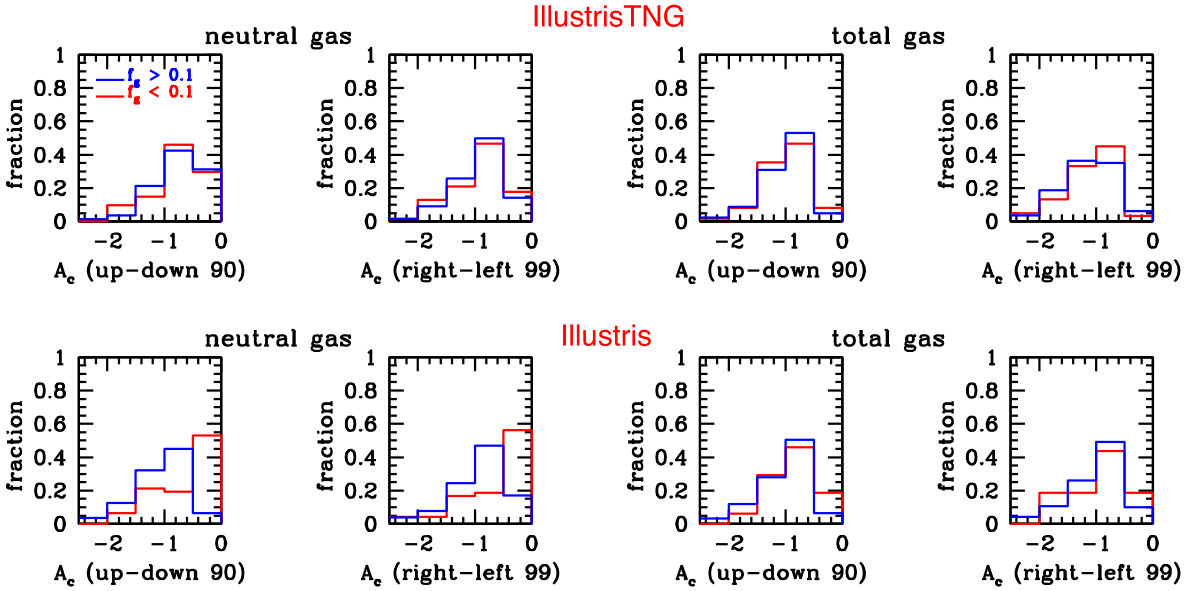

Figure 5. Comparison of two different asymmetry indices for the neutral gas distribution and the total gas distribution. Results are shown for gas-rich (f_g > 0.1; blue histograms) and gas-poor (f_g < 0.1; red histograms) galaxies. The two indices represent the asymmetry in the central gas distribution above and below the plane and the asymmetry in the far outer disc to the right and to the left of the disc minor axis. Results for IllustrisTNG are shown in the top panels and for Illustris in the bottom panels.

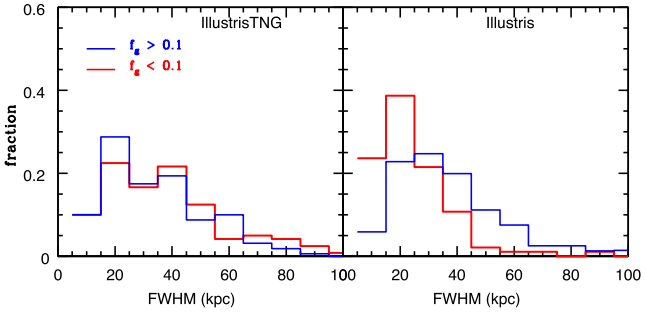

Figure 6. Histograms of the fraction of galaxies as a function of FWHM vertical extent for gas-poor galaxies with f_g < 0.1 (red) and for gas-rich galaxies with f_g > 0.1 (blue). Results are shown for IllustrisTNG in the left-hand panel and for Illustris in the right-hand panel.

galaxies have more asymmetric neutral gas distributions than gas-rich galaxies. The differences in asymmetry are much smaller for the total gas. As discussed in KBN16, the asymmetric neutral gas distributions are the effect of the bubble feedback, which acts to heat the gas and leads to irregular holes in the neutral gas distribution. In IllustrisTNG, there is no difference in CGM asymmetry between gas-rich and gas-poor galaxies.

Finally, we explore the rotational coherence scale of the CGM. Once again, we rotate the galaxy into an edge-on configuration and find the positions along the major axis, x_{min} and x_{max}, where the measured velocity reaches its maximum and minimum values. The full width half-maximum (FWHM) of the vertical coherence length of the rotation is estimated by centring at x_{min} and x_{max} and finding the distance y over which the velocity is greater than half its minimum/maximum value. The distributions of FWHM vertical extent of coherent rotation are plotted in Fig. 6 for the IllustrisTNG and Illustris gas-rich (blue) and gas-poor (red) subsamples. As can be seen, the FWHM values span the same range of values for gas-rich galaxies in the two simulations. The main difference is that there is a systematic shift towards smaller FWHM values for gas-poor galaxies in Illustris, but not in IllustrisTNG. Again, in KBN16 this trend was attributed to more vigorous bubble feedback in gas-poor galaxies, which acts to destroy coherent structures of neutral gas.

In summary, we find that large-scale CGM properties in IllustrisTNG, such as mean column density, asymmetry, and rotational coherence scale, depend much more weakly on the galaxy gas fraction than they do in Illustris. The neutral gas distribution in IllustrisTNG is also preferentially aligned in the plane of the central disc, whereas it is much more isotropic in Illustris.

4 TRACER PARTICLE ANALYSIS OF INFLOWING/OUTFLOWING AND HEATING/COOLING GAS

The equations of hydrodynamics are solved in astrophysical applications using one of the two general approaches: particle-based Lagrangian-like schemes such as smoothed particle hydrodynamics (SPH), or mesh-based Eulerian-like schemes. Lagrangian-like SPH schemes have an advantage that it is possible to follow fluid resolution elements in time and track the evolution of their properties, at the expense of introducing errors on the smoothing scale (Vogelsberger et al. 2012, section 5.3). In Eulerian-like schemes, the discretized quantity is the volume itself, and information on the past evolution of the fluid is lost. Genel et al. (2013) developed a tracer particle scheme in the moving-mesh code AREPO (Springel 2010). The scheme is based on a Monte Carlo sampling of fluid motions. Tracer particles are attached to fluid cells and whenever two cells exchange mass, they also exchange the appropriate fraction of their tracer particles. In this way, the tracer particles can be used to follow gas flows as a function of time in the simulation, with limitations due to Monte Carlo statistical noise (Nelson et al. 2013).

In this section, we compare gas temperature evolution and gas flows in Illustris and IllustrisTNG using the sample of matched subhaloes described in the previous section. The matching technique allows us to divide the full sample into a set of subsamples according

to galaxy gas fraction and still carry out meaningful comparisons using sets of around a dozen subhaloes. Our aim is to understand how the changes in the subgrid models regulating supernovae and AGN feedback impact the physical state of the CGM.

4.1 Cooling/heating and inflow/outflow balance

We begin with an examination of the balance between cooling and heating, as well as inflow and outflow in the two simulations. We work with all the gas tracer particles located within the subhaloes in our samples at $z = 0$ and extract the positions, velocities, and temperature of all these particles at a series of earlier output times. We first recentre our coordinate system to the centre of mass of the stars in the subhalo at $z = 0$. We select a region around the centre of mass within which the stellar density is larger than 2 per cent of the central stellar density and then rotate the galaxy into its edge-on configuration defined by the stellar particles. The x-axis of the new coordinate system is defined to lie along the major axis of the edge-on system, while the z-axis is perpendicular to the galactic plane. We work with the gas tracers at three different snapshot times corresponding to $z = 0.1$ ($t_{\rm look-back} = 1.3$ Gyr), 0.5 ($t_{\rm look-back} = 5.1$ Gyr), and 1 ($t_{\rm look-back} = 7.8$ Gyr). For each of these snapshots, we again recentre the tracer particles to the centre of mass of the stars and rotate them into the edge-on configuration of the inner stellar distribution at that snapshot. In this way, the bulk motion of the galaxy between the two snapshots is removed, and the motion of the gas between the two snapshots is defined with respect to the centre of mass of the disc. We define the change in radius ΔR as $\sqrt{x_1^2 + y_1^2 + z_1^2} - \sqrt{x_0^2 + y_0^2 + z_0^2}$, where (x_0, y_0, z_0) are the coordinates of the tracer particles at $z = 0$ and (x_1, y_1, z_1) are the coordinates at the earlier snapshot. If the radius has decreased between the two snapshots, we label the tracer as inflowing, and if the radius has decreased, we label it as outflowing. Tracer particles also carry the thermodynamic properties of the gas and we calculate ΔT as the difference in temperature between the two snapshots.[1] If the temperature has increased, the tracer is labelled as heating, and if it has decreased, the tracer is labelled as cooling. Note that the longer the adopted look-back time, the more likely it is that the tracers have complex behaviour within the two time windows. For gas in a fountain flow, the tracer particles could have been outflowing, then inflowing, then outflowing again, between two of our tracer time points. The quantities plotted should thus be regarded as a measure of the *net* flow averaged over many tracers within the given time window.

In the upper panels of Fig. 7, we plot the logarithm of the ratio of cooling versus heating tracer particles as a function of the distance of the particle from the centre of the subhalo at $z = 0$. In the lower panels, we plot the logarithm of the ratio of inflowing versus outflowing tracer particles as a function of radius. Note that the mean numbers of tracer particles are equivalent to 'mass', because every tracer represents a constant baryon mass. Results for IllustrisTNG are shown in the left column and in the right column for Illustris. Red, green, and blue curves are for the gas-poor, moderate gas, and gas-rich subsamples (see Section 2.2). No gas-poor results are shown for Illustris, because these are all satellite galaxies in this

[1]We note that cooling of gas is not tracked accurately below a temperature of $\sim 10^4$ K in the simulations. We have simply used the snapshot values at face value, disregarding the implementation of the Springel & Hernquist (2003) subgrid model for the interstellar medium. This means that ΔT values very close to the disc should be disregarded.

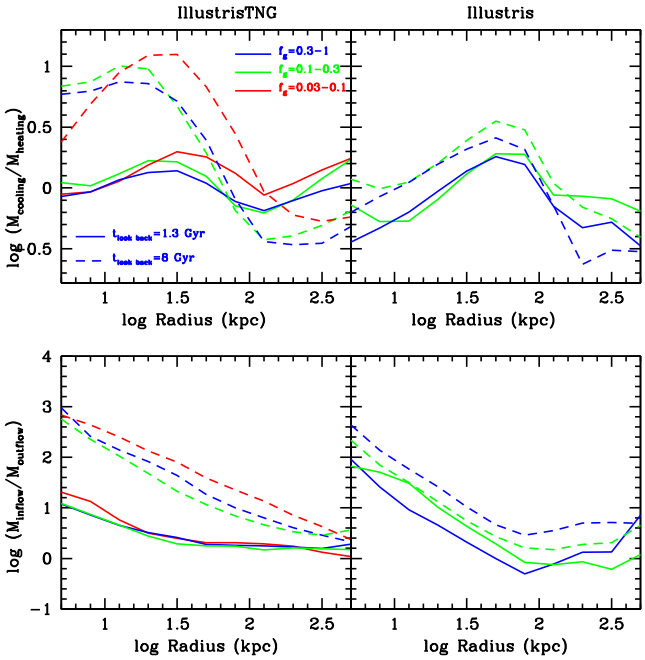

Figure 7. Upper panels: logarithm of the ratio of cooling versus heating tracer particles is plotted as a function of the distance of the particle from the centre of the subhalo at $z = 0$. Lower panels: logarithm of the ratio of inflowing versus outflowing tracer particles is plotted as a function of radius. Results for IllustrisTNG are shown in the left column and in the right column for Illustris. Red, green, and blue curves are for the gas-poor, moderate gas, and gas-rich subsamples. The solid curves show results evaluated between $z = 0.1$ and 0 (i.e. over a look-back time of 1.3 Gyr), while the dashed curves show results evaluated over a look-back time of 8 Gyr, from $z = 1$ to 0.

simulation. The solid curves show results evaluated between $z = 0.1$ and 0 (i.e. over a look-back time of 1.3 Gyr), while the dashed curves show results evaluated over a look-back time of 8 Gyr, from $z = 1$ to 0.

In IllustrisTNG, the CGM is in approximate heating/cooling equilibrium over the past 1.3 Gyr with $M_{\rm cooling} \simeq M_{\rm heating}$ all the way from the inner disc out to a radius of 100 kpc. The inflowing mass is larger than the outflowing mass out to a radius of around 30 kpc, but the CGM at larger radii is in inflow/outflow equilibrium. When evaluated over a time-scale of 8 Gyr, the picture changes quite dramatically. The cooled mass dominates over the heated mass by a factor of 10 in the inner 30–50 kpc of the halo, and approximate heating/cooling equilibrium is only reached at radii greater than 100 kpc. Likewise, the mass of gas that has flowed in over the last 8 Gyr is larger than the mass that has flowed out at all radii out to a few hundred kpc.

In Illustris, the dependence of the results on the adopted look-back time is much weaker. This means that the heating/cooling and inflow/outflow patterns in the CGM are largely *time-independent* out to $z = 1$. The inner CGM is inflow dominated, but in rough equilibrium between cooling and heating. The ratio of cooling mass over heating mass increases with radius, reaching a maximum at $R = 70$ kpc, before dropping sharply in the outer ($R > 100$ kpc) region of the halo. Likewise, the region of the halo where the inflowing mass dominates over the outflowing mass ends at $R \sim 100$ kpc, which likely indicates the region of the halo where the bubble feedback is heating the gas and pushing most of it outwards.

In summary, the results in Fig. 7 indicate a progressive decrease in the amount of cooling and inflowing gas around IllustrisTNG

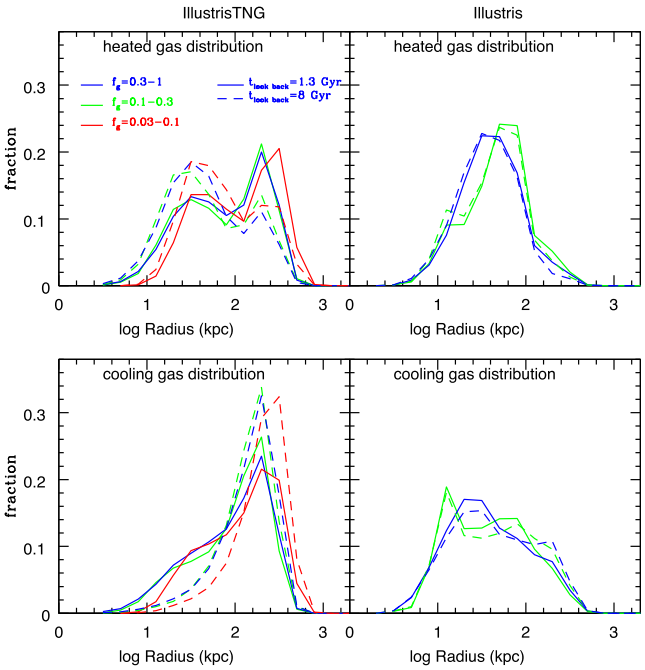

Figure 8. The distribution of the total gas mass in the halo tagged as heating or cooling as a function of radius. The format of the figure and the line styles and colours have the same meaning as in Fig. 7.

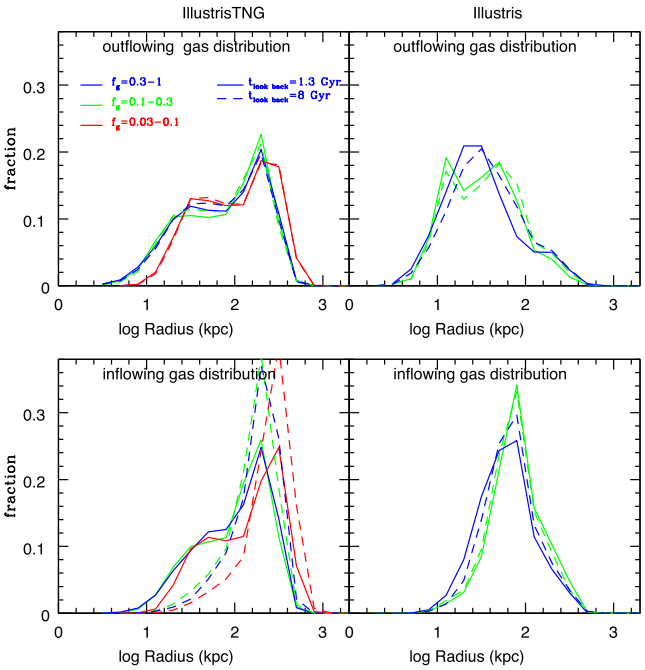

Figure 9. The distribution of the total gas mass in the halo tagged as inflowing or outflowing as a function of radius. The format of the figure and the line styles and colours have the same meaning as in Fig. 7.

Milky Way mass galaxies from $z = 1$ to 0. This occurs across the entire subhalo, but most strongly in the inner regions. In contrast, the feedback in Illustris is *time-independent*, always acting to quench the inflow of cooling gas in the outer regions of the halo. Note that these results appear to be largely independent of the present-day gas fraction of the galaxy in both simulations.

The next two figures examine how the *total gas mass in the halo* tagged as heating or cooling (Fig. 8) and as inflowing or outflowing (Fig. 9) is partitioned as a function of radius. The format of these two figures and the meanings of the different line colours and styles are the same as in Fig. 7 (see the captions for more details). In IllustrisTNG, the mass distributions tagged according to whether the tracer particles have been cooling or heating appear to be bimodal, with one part of the distribution located between 10 and 100 kpc and another one located between 100 and 400 kpc. The heated gas contributes mainly to the lower radius peak, while cooling gas is mainly located at larger distances. In Illustris, the radial separation between gas that is heated and cooled is not as pronounced. Compared to IllustrisTNG, there is a clear suppression of gas at the very largest radii, once again indicative of the effect of the bubble feedback model in pushing gas at large radii out of the subhalo. Similar conclusions are reached when the tracers are tagged according to whether they are inflowing or outflowing (Fig. 9). Illustris exhibits somewhat stronger separation in radius between the inflowing and outflowing components than between the cooling and heating components, while the opposite is true for IllustrisTNG.

Another way to think about the results presented in these two figures is in terms of the differing size-scales of the fountain flows (or of the 'baryon cycle' established by the feedback mechanisms) in the two simulations. In IllustrisTNG, there are two main flow patterns: one that is established on scales of a few tens of kpc that is maintained by a combination of supernova/AGN feedback and gravitational infall on to the central disc, and another one that is established on scales of a few hundreds of kpc that is maintained by cosmological infall and shock-heating of gas. In Illustris, the outer flow is suppressed in fractional mass contribution compared to the inner flow.

In summary, we have examined the balance between heating and cooling and inflow and outflow as a function of radius in the CGM. We have uncovered significant differences between the two simulations, indicative of the differing implementations of feedback in the two cases.

4.2 Gas accretion on to the disc

We now turn to a study of the nature of the gas that accretes on to the disc.

After rotating the galaxy into its edge-on configuration and recentring to the centre of mass of the inner stellar distribution, we define the gas disc as the radial region $r < R_{\rm max}$ in the disc plane within which the gas surface density does not drop below $1/e^2$ of its central value. We then calculate height above and below the disc plane, $z_{\rm min}$ and $z_{\rm max}$, where the gas density stays above $1/e^2$ of the average value within the gas disc. The region $r < R_{\rm max}$ and $z_{\rm min} < z < z_{\rm max}$ is defined as the 'accreted zone'. Tracer particles (either stars or gas) found within this zone at $z = 0$, which are located outside it at an earlier snapshot in the form of gas, are defined as accreted particles. In Fig. 10, we plot the temperature distribution of these tracers at earlier times, as well as their radial distribution at the earlier snapshots. The histograms have been normalized so that the sum over all bins is equal to the fraction of the $z = 0$ disc mass that has been accreted. Once again, results are shown for the two simulations in different columns. The solid curves show results for a look-back time of 1.3 Gyr and the dashed curves for a look-back time of 8 Gyr. Red, green, and blue curves indicate results for the gas-poor, moderate gas, and gas-rich subsamples, respectively.

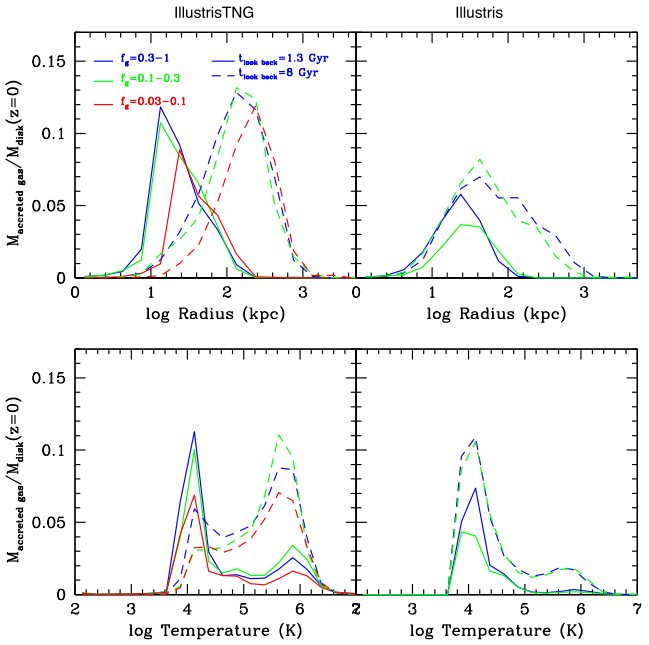

Figure 10. The radial and temperature distribution of gas particles at redshifts $z = 0.1$ (solid) and $z = 1$ (dashed) accreted on to the disc at $z = 0$. The format of the figure and the line styles and colours have the same meaning as in Fig. 7.

In both Illustris and IllustrisTNG, gas-rich galaxies have undergone more accretion than gas-poor galaxies. In Illustris, this trend is only seen for recent look-back times, but in IllustrisTNG, this persists for look-back times out to $z = 1$. We also see that in Illustris, the majority of the accretion is in the form of relatively cool gas, when evaluated over long look-back times. In contrast, in IllustrisTNG, recent accretion is from cool gas located at radii between 10 and 100 kpc from the disc, but when evaluated over look-back times of 8 Gyr, we see that much of the accreted material was hot with temperatures $\sim 10^6$ K at $z = 1$ and that at this redshift, this gas was located between 100 kpc and 1 Mpc from the disc. We note that the trend in CGM accreted fraction with galaxy gas fraction is quite small; this implies that the subsequent conversion rate of gas into stars in the disc is likely playing a significant role in setting the observed present-day gas fraction of the galaxy in both simulations.

To summarize, Figs 8, 9, and 10 show that accretion in Illustris is dominated by a small-scale (10–50 kpc) fountain flow of mainly cold material. This is consistent with the conclusions of Nelson et al. (2015b), who showed that accretion in Illustris is dominated by recycled material out to redshifts $\sim$1. In TNG, however, the longer time-scale picture is accretion of hotter gas from larger distances. This implies a different balance between hot gas cooling from the halo and cool, recycled fountain gas as the accretion source for the galaxy.

The strong evolution of cooling/accretion with redshift in TNG compared to Illustris can likely be attributed to different redshift evolution of wind properties. The right-hand panels of figs 6 and 7 of Pillepich et al. (2018) show that the evolution of the wind mass-loading factor and velocity at injection with redshift actually have different behaviours. In dark matter haloes with masses 10^{12} $M_\odot$ in TNG, the wind velocity at injection remains constant at a value of $\sim$1000 km s^{-1} from $z = 4$ to 0 in TNG, while the wind mass-loading factors decrease by a factor of 2 from 4 to 2 over this redshift range. This implies that SN feedback evolves only weakly with redshift. The likely explanation for the strong evolution in CGM properties with redshift in this simulation is strongly evolving AGN feedback, as the galaxy transitions into the kinetic mode at the threshold mass. In Illustris, the wind velocity decreases from 700 km s^{-1} at $z = 4$ to 400 km s^{-1} at $z = 0$, while the wind mass-loading factors increase from 2 to 4.5 over the same redshift range. These opposing trends, combined with the fact that AGN feedback affects gas mainly at large distances in the halo, may offer an explanation for why CGM properties in this simulation are so invariant with redshift.

4.3 How does the CGM differ between gas-rich and gas-poor galaxies?

It is reasonable to suppose that way to pinpoint why some galaxies are gas-rich and some galaxies are gas-poor is by separating the CGM gas into different thermodynamic and kinematic components as a function of radius.

In Figs 11 and 12, we show how tracer particles in the CGM are partitioned within the space of ΔR versus ΔT, where ΔR is the change in radius of the particles, with negative values indicating inflow and positive values indicating outflow, and ΔT is the change in temperature, with negative values indicating cooling and positive values indicating heating. Results for the inner CGM (radii less than 30 kpc) are shown in Fig. 11 and for the outer CGM (radii greater than 30 kpc) are shown in Fig. 12. We have adopted a tracer time interval of 5 Gyr for the inner CGM and 8 Gyr for the outer CGM. In both the figures, IllustrisTNG results for three gas fraction subsamples are presented in the left columns, while the right columns show results for the two Illustris subsamples. The contour spacing in each panel is 0.4 dex in the logarithm of the fraction of the total number of particles; the lowest contour level (plotted in black) corresponds to log $F = -4.9$ and the highest contour level (plotted in white) corresponds to log $F = -1.2$.

In each panel in the two figures, there are four distinct quadrants corresponding to (a) cooling gas that is inflowing (lower left), (b) cooling gas that is outflowing (upper left), (c) heated gas that is inflowing (lower right), and (d) heated gas that is outflowing (upper right). The sum over all four quadrants is renormalized to 1, so that comparisons between the different panels can be made in a meaningful way. Symmetry between positive and negative values on the ΔT and ΔR axes would indicate that the gas is in thermal and inflow/outflow equilibrium, respectively. In agreement with the results shown in Fig. 7, we see that on small scales, gas is strongly inflowing and cooling in IllustrisTNG. In Illustris, gas is inflowing but is in rough thermal equilibrium. On large scales, the inflowing gas is in thermal equilibrium in both the simulations, as expected since most gas is virialized within the halo and cooling times are long. The outflowing gas component, on the other hand, is experiencing net heating in IllustrisTNG, but net cooling in Illustris, which presumably reflects the different subgrid models for feedback in the two simulations.

In IllustrisTNG, the most striking change as a function of the gas mass fraction of the galaxy is that there is a clear increase in the fraction of gas present in the heated, inflowing component on small scales for more gas-rich systems. In Illustris, the most striking change in the CGM surrounding galaxies of different gas mass fractions occurs in the outer regions. Gas-poor systems have more mass (both material that is cooling and being heated) in an outflowing component.

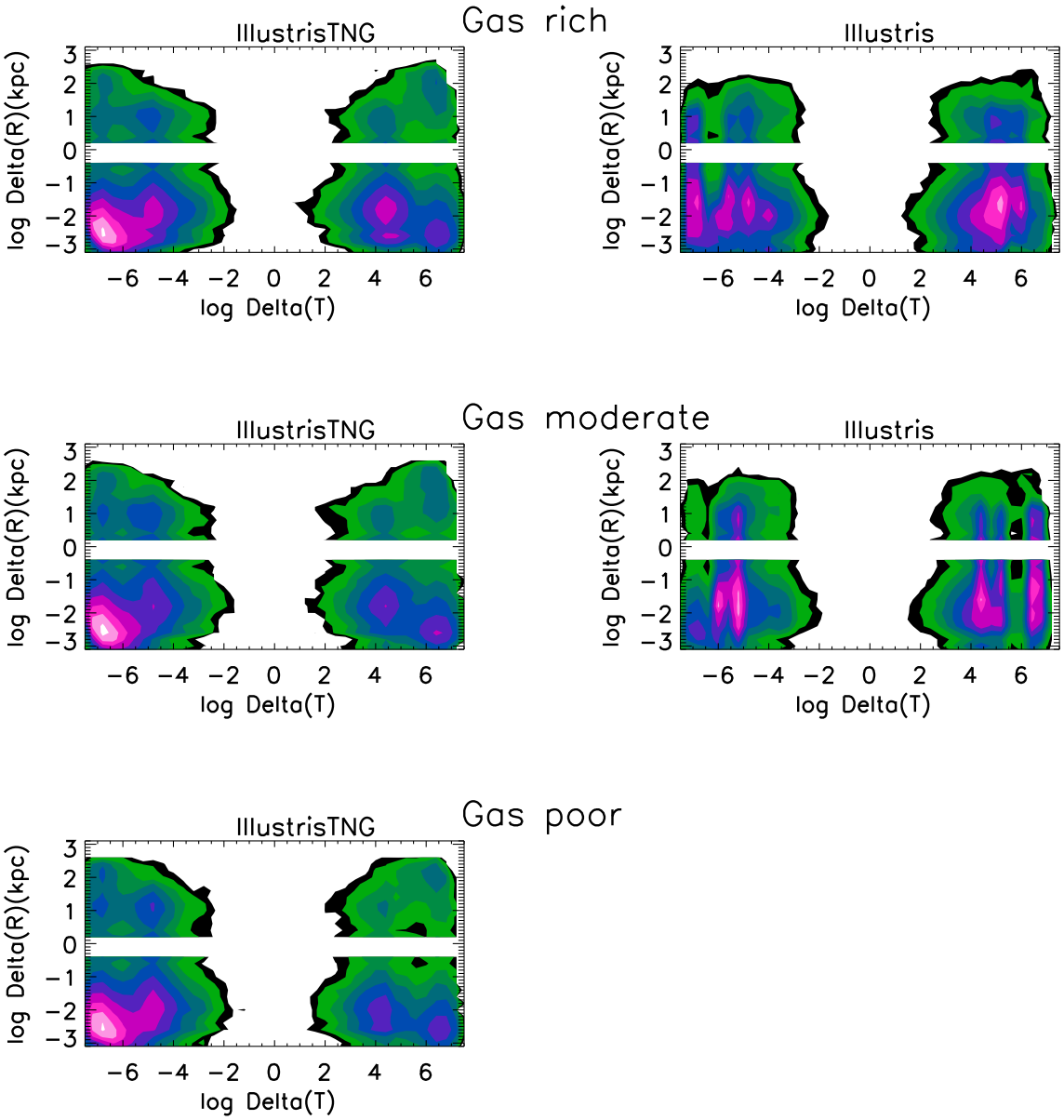

Figure 11. The distribution of tracer particles in the CGM within 30 kpc from the centre of the subhalo in the two-dimensional plane of ΔR versus ΔT, where ΔR is the change in radius of the particles, with negative values indicating inflow and positive values indicating outflow, and ΔT is the change in temperature between $z = 0.5$ and 0, with negative values indicating cooling and positive values indicating heating. The contour spacing in each panel is 0.4 dex in the logarithm of the fraction of the total number of particles within the radius; the lowest contour level (plotted in black) corresponds to $\log F = -4.9$ and the highest contour level (plotted in white) corresponds to $\log F = -1.2$. Results are shown for three different gas fraction subsamples for IllustrisTNG and two different ones for Illustris.

To summarize, we find that the reservoir that varies most with the gas fraction of a galaxy is distributed over very different scales in the two simulations. In IllustrisTNG, the reservoir is in the form of heated, galactic fountain gas on scales of a few tens of kpc that later re-accretes on to the central system. In Illustris, the feedback energy is dumped at larger distances from the central system, and the gas fraction is regulated by how much of the large-scale (∼100 kpc) gas reservoir is able to cool and re-accrete over long time-scales.

4.4 Example of a gas-rich galaxy in both simulations

To illustrate the different gas components in a pictorial fashion, we select matched subhaloes in the gas-rich subsamples of Illustris and IllustrisTNG, and plot the tracer particles. Figs 13 (IllustrisTNG) and 14 (Illustris) show the tracers in edge-on and face-on configurations for one typical matched subhalo in the gas-rich subsample. The upper panels show the inner region of the disc, limited to a radius of 20 kpc at $z = 0$, while the lower panels show a larger scale view of where the same particles were located at $z = 0.5$. The tracer particles have been colour coded according to whether they have experienced heating/cooling or inflow/outflow between $z = 0.5$ and 0: blue indicating particles that are cooling and inflowing, green indicating particles that have been heated but have flowed into the central disc, yellow indicating material that has cooled but is outflowing, and red indicating material that is heated and outflowing.

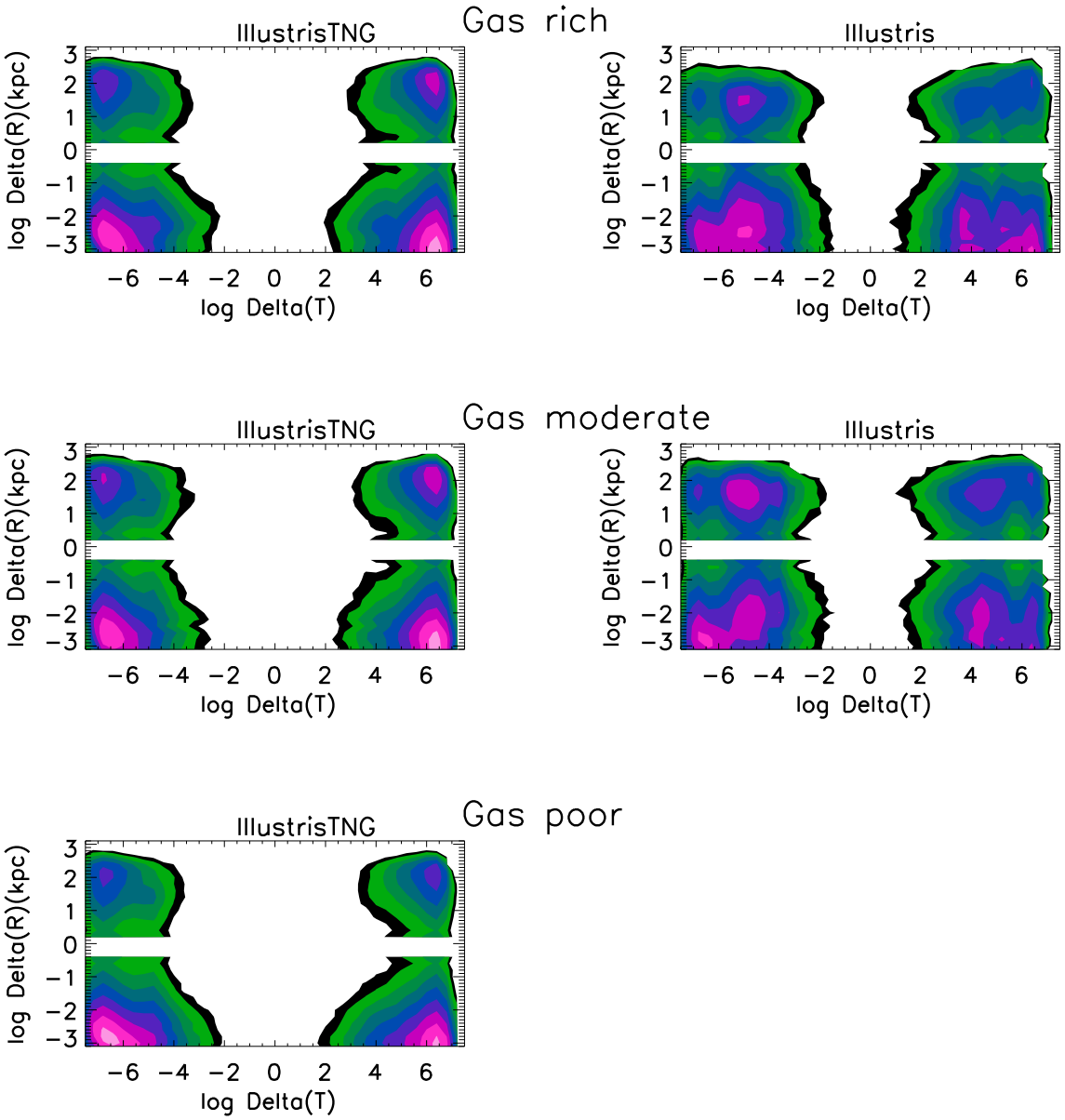

Figure 12. As in the previous figure, except for tracer particles in the CGM further way than 30 kpc from the centre of the subhalo. ΔR and ΔT are evaluated between $z = 1$ and 0.

There are a number of very striking differences between the simulations, which we will now discuss. The reader should recall that matched subhaloes originate from the same patch of particles in the initial conditions of the two simulations and therefore the dark matter merger histories will be close to identical, since gravitational forces are dominated by the dark matter component and not the baryons. The differences between Figs 13 and 14 should largely reflect the changes in the prescriptions for supernova and AGN feedback in the two simulations, modulo any 'timing offset' caused by the fact that the two systems might be in slightly different evolutionary stages in the two runs as a result of the differences in the treatment of the baryonic physics and the small difference in cosmological parameters in the two simulations. Comparison of the top two panels in the two figures shows that the gas is much more extended perpendicular to the disc in Illustris, in agreement with our finding in Section 3, and that Illustris gas-rich discs have large vertical coherence lengths. The distribution of the gas away from the disc mid-plane is not uniform, but exhibits large bubble-like structures, which are likely tidal debris remnants rather than AGN feedback signatures, because most of the gas in the vertically extended part of the disc is cold and inflowing. In both the simulations, the heated gas is always located in denser-than-average structures in the disc, indicating that the heated gas traces regions where stars are forming more rapidly. The heated, outflowing gas is located at larger radius in the disc than the heated, inflowing gas, as expected. In Illustris, heated, outflowing gas also contributes to the vertically extended gas component at the largest scale heights above the disc plane.

Moving to the lower panels of Figs 13 and 14, we see that in IllustrisTNG, a significant fraction of the disc has cooled and condensed from a smooth, rather uniform reservoir of material extending out to radii of around 150 kpc. Most of the heated,

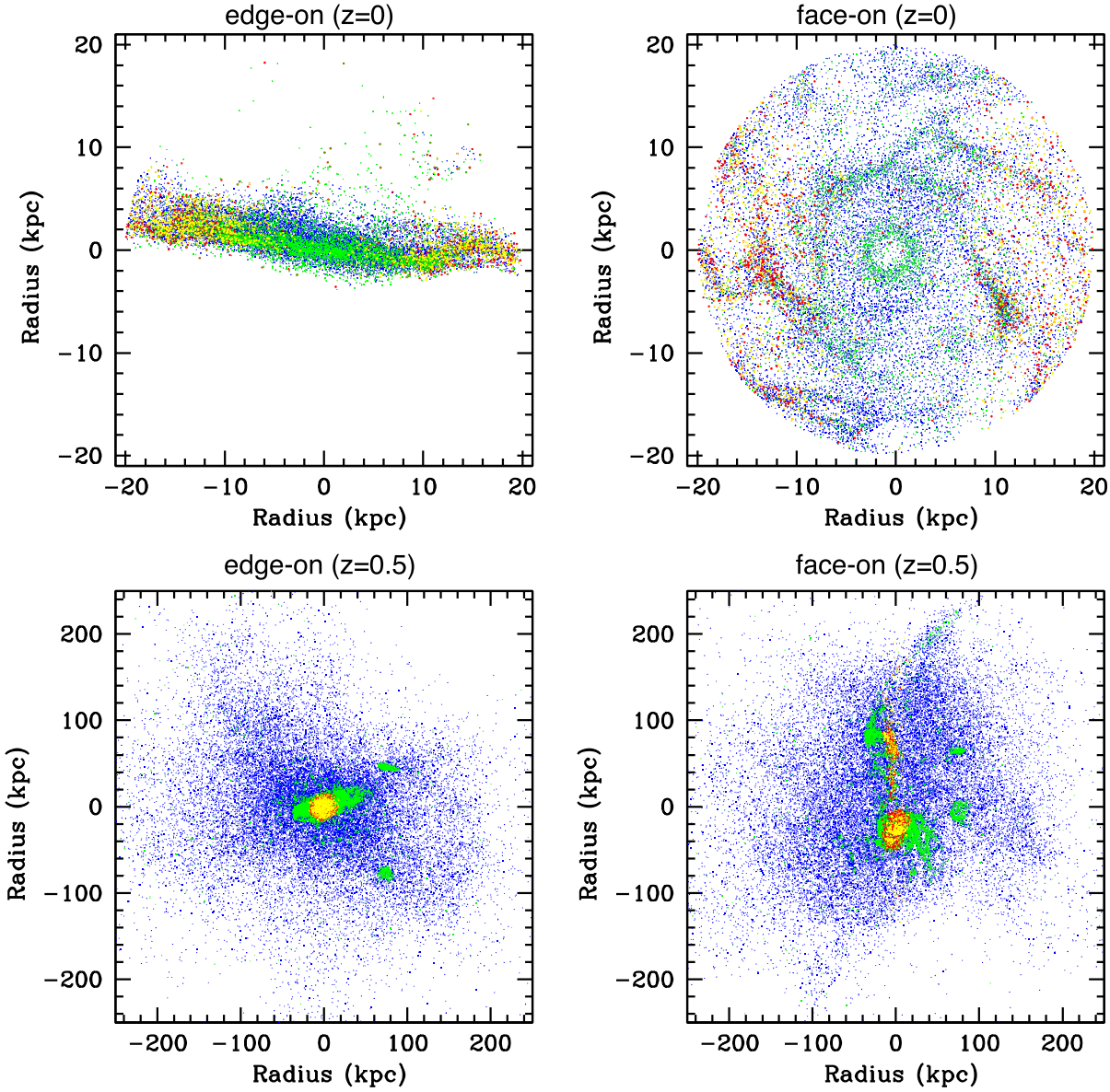

Figure 13. Tracer particles in one gas-rich galaxy in IllustrisTNG are plotted in edge-on and face-on configurations. The upper panels show the inner region of the disc, limited to a radius of 20 kpc at $z = 0$, while the lower panels show a larger scale view of where the same particles were located at $z = 0.5$. The tracer particles have been colour coded according to whether they have experienced heating/cooling or inflow/outflow between $z = 0.5$ and 0: blue indicating particles that are cooling and inflowing, green indicating particles that have been heated but have flowed into the central disc, yellow indicating material that has cooled but is outflowing, and red indicating material that is heated and outflowing.

inflowing gas is located in a flattened structure of around 80 kpc in diameter. A smaller fraction is located in satellite systems that are destined to merge with the main disc. The outflowing gas is the most centrally concentrated. In contrast, the gas distribution at $z = 0.5$ in Illustris is contained in 3–4 much more massive structures and there is very little smooth reservoir. The gas disc has thus grown through a series of merging events, which explains why the present-day disc is considerably more irregular than in IllustrisTNG and also exhibits a strong bar.

In summary, in the most gas-rich galaxies in IllustrisTNG, feedback processes have acted at high redshifts to drive a significant fraction of the gas into a smooth, quasi-spherical halo-like structure, which then condenses to form a thin disc at low redshifts. In IllustrisTNG, much of the gas is accreted recently in the form of clouds of recycled material, which merge in a configuration that creates a thickened, rotating structure.

5 SUMMARY AND FUTURE PERSPECTIVES

The goals of this analysis were twofold: (a) to understand the extent to which the conclusions drawn in KBN16 about trends in structure and kinematics of the CGM as a function of galaxy gas mass fraction are dependent on the adopted prescription for supernovae and AGN feedback in the simulations; (b) to understand how structural and kinematic trends reflect underlying physical processes at work in the CGM, namely cooling and inflow of gas on to the galaxy under gravity as the surrounding dark

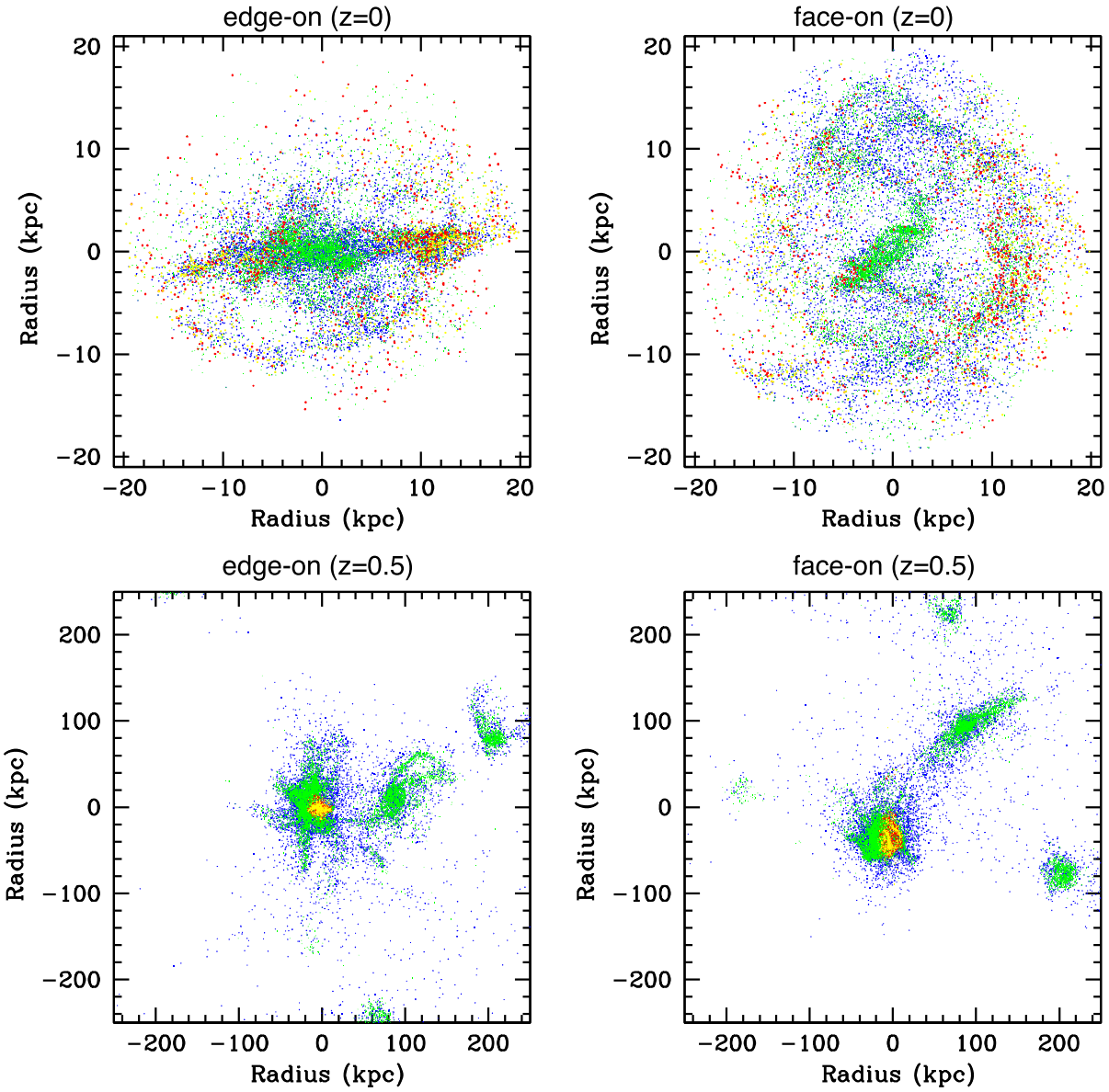

Figure 14. As in Fig. 13, for the tracer particles in the matched subhalo in Illustris.

matter halo assembles over time, as well as heating and outflow of gas as a result of energy ejection by stellar and black hole sources.

The answer to the first investigation is that all the trends identified in KBN16 are no longer present in IllustrisTNG. For our sample of Milky Way mass haloes at $z = 0$, gas column density and temperature profiles at large radii ($\sim$100 kpc) no longer correlate with the gas mass fraction of the central galaxy in IllustrisTNG. The neutral gas at large radii is preferentially aligned in the plane of the disc in IllustrisTNG, whereas it is much more isotropic in Illustris. There is also no longer any relation between asymmetries in the neutral gas distribution and galaxy gas mass fraction. Finally, the vertical coherence scale of the rotationally supported gas in the CGM is also no longer linked to the gas mass fraction of the galaxy.

Our tracer particle analysis allows us to construct a fairly detailed physical picture to explain why the differences between the simulations are so striking. In IllustrisTNG, there is a very strong redshift dependence in the properties of the CGM. The CGM at $z = 1$ is very strongly cooling and inflow dominated, and then evolves to a state where heating/cooling and inflow/outflow rates roughly balance each other at $z = 0$. In contrast, there is little redshift evolution of CGM properties out to $z = 1$ in Illustris.

When we look in detail at the morphology of the material that has cooled to form the galactic disc in Illustris, we find that it is located in a smoothly distributed, isotropic halo of gas that has cooled from temperatures of $\sim 10^5$–10^6 K at $z = 1$ to 10^4 K at the present day. In contrast, the material that has formed the disc in Illustris is already in the form of lumps of cool ($\sim 10^4$–10^5 K) gas at $z = 1$. These results can be understood by considering the very different way in which feedback operates in the two simulations. In IllustrisTNG, kinetic feedback operates efficiently near the centres of galaxies at high redshifts to drive gas out of these systems (i.e. the winds have high mass-loading factors). This reservoir of smooth material cools

and collapses to form a thin, rotating disc by the present day. In Illustris, the feedback energy is dumped at large radii by heating the gas in large 'bubbles', which pushes a significant fraction of the hot gas out of the halo. The cooler lumps merge, forming a more vertically thickened structure.

Finally, when we look at how the gas is partitioned into inflowing/outflowing and heating/cooling components as a function of radius around galaxies of different gas mass fractions, we are able to understand in more detail how the CGM is regulating the gas supply to the disc in both simulations. In IllustrisTNG, the regulation to the disc occurs on smaller scales than in Illustris. Gas-rich galaxies have a larger fraction of inflowing heated gas on scales of a few tens of kpc that maintains the gas supply to the galaxy. In contrast, the galaxy gas fraction in Illustris depends on the degree to which bubble feedback has managed to empty the halo on larger scales. In short, IllustrisTNG galaxies are fuelled by 'galactic fountains', while the gas supply for Illustris galaxies is regulated on much larger scales by processes that heat and remove the gas from their haloes.

Perhaps the most striking and unexpected result from this work is the degree to which the low-redshift CGM is dependent on the detailed implementation of supernova and AGN feedback processes in the simulated galaxies, most of which reach their peak efficiency at redshifts greater than 1. Much effort is now being invested in characterizing outflows from high-redshift star-forming and active galaxies (e.g. Davies et al. 2019); our results suggest that checks on observed parametrizations of velocities and mass-loading factors of outflowing gas from star-forming galaxies (Nelson et al. 2019) should be complemented by systematic characterization of the structure and kinematics of gas around low-redshift galaxies to ensure that a consistent picture emerges from the simulations. As discussed in KBN16, this can be done in a number of ways, including quasar absorption line statistics (Tumlinson et al. 2013; Werk et al. 2014; Borthakur et al. 2015), radio interferometric studies of H I around galaxies (e.g. Wang et al. 2014), deep observations of extra-planar, diffuse ionized gas using integral field unit spectra (e.g. Jones et al. 2017) and X-ray and Sunyaev–Zeldovich studies of hot gas haloes around galaxies (e.g. Anderson et al 2015).

The fact that no systematic trends in CGM properties are found as a function of galaxy gas mass fraction in IllustrisTNG in contradiction with the results of Borthakur et al. (2015) would appear to indicate that further tuning of the feedback recipes will be required to match observations in detail. Kauffmann, Borthakur & Nelson (2016) showed that even though the observed disc gas fraction distributions agree well with Illustris, the covering fraction of neutral gas is a factor of 2 smaller than the data at large radii in the haloes. This is attributed to the radio-mode feedback heating gas to high temperatures at large radii from the central source. Nelson et al. (2018a,b) show that the gas covering fraction problems discussed in this paper are alleviated in IllustrisTNG. The remaining issue is whether the strong alignment of neutral gas with the H I disc is inconsistent with data. The main problem is that the Borthakur absorber sample currently consists of only 45 galaxies that have stellar masses uniformly distributed between 10^{10} and 10^{11} $M_\odot$. By construction, the feedback physics in the simulations changes strongly across this mass range. In all simulations, this is necessary in order to match the transition from a predominantly blue population of galaxies at 10^{10} $M_\odot$ to a predominantly red population of galaxies at 10^{11} $M_\odot$. In future, analysis of larger galaxy samples and continued dialogue between observations and simulations will hopefully yield a reasonably complete answer to the puzzle of how galaxies acquire their gas.

ACKNOWLEDGEMENTS

We thank Volker Springel, Shy Genel and Paul Torrey for helpful comments on the manuscript.

REFERENCES

Anderson M. E., Gaspari M., White S. D. M., Wang W., Dai X., 2015, MNRAS, 449, 3806
Arrigoni Battaia F., Prochaska J. X., Hennawi J. F., Obreja A., Buck T., Cantalupo S., Dutton A. A., Macciò A. V., 2018, MNRAS, 473, 3907
Bauermeister A., Blitz L., Ma C.-P., 2010, ApJ, 717, 323
Borthakur S. et al., 2015, ApJ, 813, 46
Danovich M., Dekel A., Hahn O., Ceverino D., Primack J., 2015, MNRAS, 449, 2087
Davies R. L. et al., 2019, ApJ, 873, 122
Diemer B. et al., 2018, ApJS, 238, 33
Dubois Y., Volonteri M., Silk J., 2014, MNRAS, 440, 1590
Genel S. et al., 2014, MNRAS, 445, 175
Genel S., Vogelsberger M., Nelson D., Sijacki D., Springel V., Hernquist L., 2013, MNRAS, 435, 1426
Genzel R., Eisenhauer F., Gillessen S., 2010, Rev. Mod. Phys., 82, 3121
Ho S. H., Martin C. L., Kacprzak G. G., Churchill C. W., 2017, ApJ, 835, 267
Jones A. et al., 2017, A&A, 599, A141
Kacprzak G. G., Churchill C. W., Nielsen N. M., 2012, ApJ, 760, L7
Kauffmann G., Borthakur S., Nelson D., 2016, MNRAS, 462, 3751
Khandai N., Di Matteo T., Croft R., Wilkins S., Feng Y., Tucker E., DeGraf C., Liu M.-S., 2015, MNRAS, 450, 1349
Liu G., Zakamska N. L., Greene J. E., Nesvadba N. P. H., Liu X., 2013, MNRAS, 430, 2327
Lovell M. R., Frenk C. S., Eke V. R., Jenkins A., Gao L., Theuns T., 2014, MNRAS, 439, 300
Marinacci F. et al., 2018, MNRAS, 480, 5113
Martin D. C., Matuszewski M., Morrissey P., Neill J. D., Moore A., Steidel C. C., Trainor R., 2016, ApJ, 824, L5
Martin C. L., Ho S. H., Kacprzak G. G., Churchill C. W., 2019, preprint (arXiv:1901.09123)
Naiman J. P. et al., 2018, MNRAS, 477, 1206
Nelson D., Vogelsberger M., Genel S., Sijacki D., Kereš D., Springel V., Hernquist L., 2013, MNRAS, 429, 3353
Nelson D. et al., 2015a, Astron. Comput., 13, 12
Nelson D., Genel S., Vogelsberger M., Springel V., Sijacki D., Torrey P., Hernquist L., 2015b, MNRAS, 448, 59
Nelson D. et al., 2018a, MNRAS, 477, 450
Nelson D. et al., 2018b, MNRAS, 475, 624
Nelson D. et al., 2019, preprint (arXiv:1902.05554)
Oppenheimer B. D., 2018, MNRAS, 480, 2963
Oppenheimer B. D., Davé R., 2006, MNRAS, 373, 1265
Pakmor R. et al., 2017, MNRAS, 469, 3185
Pakmor R., Springel V., 2013, MNRAS, 432, 176
Pakmor R., Bauer A., Springel V., 2011, MNRAS, 418, 1392
Pillepich A. et al., 2018, MNRAS, 473, 4077
Putman M. E., Peek J. E. G., Joung M. R., 2012, ARA&A, 50, 491
Rix H.-W., Bovy J., 2013, A&AR, 21, 61
Schaye J. et al., 2015, MNRAS, 446, 521
Sijacki D., Springel V., Di Matteo T., Hernquist L., 2007, MNRAS, 380, 877
Springel V. et al., 2018, MNRAS, 475, 676
Springel V., 2010, MNRAS, 401, 791
Springel V., Hernquist L., 2003, MNRAS, 339, 289
Stevens A. R. H. et al., 2019, MNRAS, 483, 5334
Stevens A. R. H., Lagos C. d. P., Contreras S., Croton D. J., Padilla N. D., Schaller M., Schaye J., Theuns T., 2017, MNRAS, 467, 2066
Stewart K. R. et al., 2017, ApJ, 843, 47
Stewart K. R., Kaufmann T., Bullock J. S., Barton E. J., Maller A. H., Diemand J., Wadsley J., 2011, ApJ, 738, 39

Suresh J., Bird S., Vogelsberger M., Genel S., Torrey P., Sijacki D., Springel V., Hernquist L., 2015, MNRAS, 448, 895
Tumlinson J. et al., 2013, ApJ, 777, 59
Vogelsberger M. et al., 2014a, MNRAS, 444, 1518
Vogelsberger M. et al., 2014b, Nature, 509, 177
Vogelsberger M., Sijacki D., Kereš D., Springel V., Hernquist L., 2012, MNRAS, 425, 3024
Wang J. et al., 2014, MNRAS, 441, 2159
Weinberger R. et al., 2017, MNRAS, 465, 3291
Weinberger R. et al., 2018, MNRAS, 479, 4056
Werk J. K. et al., 2014, ApJ, 792, 8
Zhu G. et al., 2014, MNRAS, 439, 3139

This paper has been typeset from a TEX/LATEX file prepared by the author.